HHS Public Access

Author manuscript

Angew Chem Int Ed Engl. Author manuscript; available in PMC 2019 July 09.

Published in final edited form as:

Angew Chem Int Ed Engl. 2018 July 09; 57(28): 8463–8467. doi:10.1002/anie.201802351.

Synchronous Chemoradiation Nanovesicles by X-ray Triggered Cascade of Drug Release

Dr. Zijian Zhou[*], **Mr. Alexander Chan**, **Dr. Zhantong Wang**, **Mr. Xiaolin Huang**, **Dr. Guocan Yu**, **Dr. Orit Jacobson**, **Dr. Sheng Wang**, **Dr. Yijing Liu**, **Dr. Lingling Shan**, **Dr. Yunlu Dai**, **Dr. Zheyu Shen**, **Dr. Lisen Lin**, **Dr. Wei Chen**, and **Dr. Xiaoyuan Chen**[*]

[*]Laboratory of Molecular Imaging and Nanomedicine, National Institute of Biomedical Imaging and Bioengineering, National Institutes of Health, Bethesda, MD 20892, USA

Abstract

Concurrent chemoradiation therapy has gained acceptance as a standard of care for treating many types of cancer in clinic due to the potential of synergism. Here, we advanced the approach of concurrent to synchronous chemoradiation by well-designed nanovesicles permitting X-ray irradiation-triggered instant drug release. The nanovesicles consist of Au nanoparticles tethered with irradiation labile linoleic acid hydroperoxide (LAHP) molecules and oxidation-responsive poly(propylene sulfide)-poly(ethylene glycol) (PPS-PEG) polymers, where DOX were loaded in the inner core of the vesicles (Au-LAHP-vDOX). Upon irradiation, the in situ formation of hydroxyl radicals (•OH) from LAHP molecules triggers the internal oxidation of PPS from being hydrophobic to hydrophilic, leading to degradation of the vesicles and burst release of cargo drugs. In this manner, synchronous chemoradiation showed impressive anticancer efficacy both in vitro and in a subcutaneous mouse tumor model by one-dose injection and one-time irradiation.

Graphical Abstract

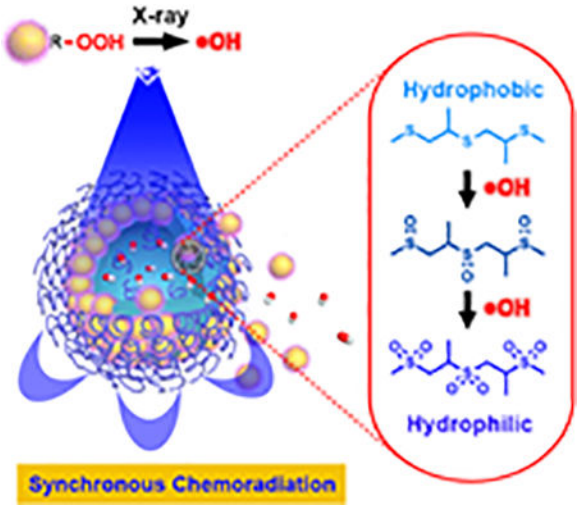

Supporting information for this article is available on the WWW under http://dx.doi.org/10.1002/anie.201xxxxxx

Synchronous Chemoradiation Nanovesicles were developed by X-ray triggered cascade of drug release, which showed impressive anticancer efficacy both *in vitro* and in a subcutaneous mouse tumor model by one-dose injection and one-time irradiation.

Keywords

chemoradiation; cancer therapy; nanovesicles; drug release; oxidation responsive

Combination therapy promises great clinical impact due to the additive and even synergistic efficacies between different treatment mechanisms. There are more than 10,000 ongoing clinical trials registered in the US regarding combination therapy of a wide variety of diseases, such as infectious diseases, neurological disorders, and cancers.[1] Particularly, successful cancer therapy requires rational design of anticancer strategy in which combination therapy holds great promise.[2] Various treatment options can be applied in combination depending on cancer types and stages, such as chemotherapy combos and chemoradiation therapy.[3] The latter is known as a logical and reasonable approach which combines the advantages of spatial control of radiotherapy and systemic survival of chemotherapy together to effectively cure cancers. It is evidenced in clinical trials that combination chemoradiation therapy leads to enhanced overall survival of patients for many solid tumors.[4] While combining chemotherapy and radiotherapy can be deployed by either concurrent procedure or sequential workflow, concurrent chemoradiation is superior to sequential strategy with significantly higher survival rates.[4a] Therefore, concurrent chemoradiation is emerging as a standard of care for treating many locally advanced tumors in the clinic, potentiating the approach of simultaneously introducing dual treatments in a confined manner.[5] However, concurrent chemoradiation by applying radiotherapy during the period of chemotherapy timespan is still underrepresented due to their disparate tempos of action.

Modern nanomedicine has provided numerous platforms incorporating exceptional nanocarriers and traditional anticancer strategies for improved cancer therapy.[6] Moreover, stimuli-responsive systems for on-demand triggered drug release have gained momentum,[7] by which cancer therapy may benefit greatly from the enhanced drug utilization and reduced systemic side effects.[8] For example, one can design a labile structure which is specifically responsive to certain internal stimuli in tumor microenvironment,[9] such as pH, reducibility, and reactive oxygen species (ROS).[10] Alternatively, extrinsically controllable drug releasing mechanisms by external stimuli hold great promise in spatiotemporal management of cancer therapy.[11] External beam radiation therapy applies high-energy X-rays to exert direct ionization damage to organelles as well as promoting intracellular ROS level. However, the use of X-ray irradiation as an external stimulus to trigger drug release in chemoradiation therapy is rarely studied.[12] It is conceivable that integrating ROS responsive materials may provide a mechanistic way of X-ray triggered drug release, yet this strategy needs careful consideration on the limited lifetime and short diffusion distance of ROS generated upon irradiation.[13]

Herein, we present a rational design of nanovesicles featuring X-ray activatable drug release for synchronous chemoradiation. The nanovesicles were fabricated by self-assembly of ROS responsive poly(propylene sulfide)-poly(ethylene glycol) (PPS-PEG) amphiphilic polymers and hydrophobic Au nanoparticles (Au NPs) tethered with X-ray labile linoleic acid hydroperoxide (LAHP) molecules (Figure 1). Hydrophilic drugs doxorubicin hydrochloride (DOX) were loaded in the inner core of the vesicles (denoted as Au-LAHP-vDOX). It is noted that PPS-PEG polymers are stable at the low biologically relevant level of ROS (1–1000 μM),[14] due to the limited diffusion and penetration of ROS in aqueous surroundings into the hydrophobic PPS backbones.[15] One highlight of our system is that the heterolysis of hydroperoxide bond in LAHP upon X-ray irradiation leads to localized formation of hydroxyl radical (•OH) within the PPS membrane. Subsequently, the *in situ* oxidation of PPS from hydrophobic thioether to sulfoxide and finally hydrophilic sulfone results in efficient degradation of the Au-LAHP-vDOX and release of cargo drugs.[16] In this manner, drug release is synchronously confined when radiation therapy is applied, which may largely mitigate possible development of resistance to monotherapy and in turn potentiate the maximal synergism in chemoradiation therapy.[17] Meanwhile, this approach may also benefit from the radiation dose enhancement effect by the high atomic number (Z) Au NPs and the ROS mediated mechanisms for improving treatment outcomes.[18]

We first synthesized PPS-PEG copolymers following a modified procedure from literature (Supporting Information, Figure S1-S4),[19] which self-assembled into vesicular structure with a size of about 80–90 nm (Figure 2a). The membrane thickness of the PPS-PEG vesicles was estimated to be around 6–8 nm according to transmission electron microscopy (TEM) images. Au NPs with a diameter of 5 nm were modified with LAHP motifs through a ligand exchange procedure (Supporting Information, Figure S5 and S6). Meanwhile, hydrophilic drugs DOX were introduced into the inner space of the vesicles during the self-assembly, denoted as Au-LAHP-vDOX, which showed a diameter of around 80 nm from TEM image (Figure 2b). A slight decrease of the hydrodynamic diameters for vesicles was observed after incorporation with Au NPs, and a broad absorption spectrum for Au vesicles was recorded (Supporting Information, Figure S7). For comparison purposes, different formulations including DOX loaded polymer only vesicles (vDOX), Au-LAHP-v, and non-responsive linoleic acid (LA) based vesicles (Au-LA-vDOX) were also prepared (Supporting Information, Figure S8).

The drug loading content in the vDOX was measured to be 14.7 wt% (weight percentage) under a theoretical DOX loading content of 25 wt%. In the presence of Au NPs, the DOX loading contents in Au-LA-vDOX and Au-LAHP-vDOX formulations were 7.8 wt% and 8.3 wt%, respectively, under a theoretical DOX loading content of about 16.7 wt%. We further tested the ability of LAHP in the formation of •OH under X-ray irradiation using 3,3’,5,5’-tetramethylbenzidine (TMB) as an indicator. We show that, under a radiation dose of 8 Gy at a voltage of 217.5 kV, both LAHP and H_2O_2 were able to oxidize TMB resulting in blue solution, whereas the TMB aqueous solution alone did not show obvious color change (Supporting Information, Figure S9).

To study the drug releasing profiles, Au-LAHP-vDOX and Au-LA-vDOX were applied with X-ray irradiation (8 Gy, denoted as + hereafter) and the cumulative drug release was

calculated at different time points. After irradiation, we incubated these formulations in either PBS (1×) or H_2O_2 (100 μM) solution in which the later was used to mimic the oxidative environment in biological systems. In both solutions, Au-LAHP-vDOX exhibited a burst release of DOX within the first 30 min after irradiation, up to 46.7% and 52.2% in PBS and H_2O_2 solutions, respectively (Figure 2c). Remarkably, the drug release of the Au-LAHP-vDOX incubated in H_2O_2 gradually increased to 76.7% at 24 h post-irradiation, whereas the late-time drug release in PBS was minimal. In contrast, the drug release of the Au-LA-vDOX showed little to no response to X-ray irradiation. Parallel studies further revealed that there were negligible differences between drug release profiles in H_2O_2 and PBS for samples without irradiation (Supporting Information, Figure S10). Moreover, the physiological stability of these DOX loaded vesicles (e.g., vDOX, Au-LA-vDOX, and Au-LAHP-vDOX) were further confirmed in the plasma, which showed negligible drug release and change of hydrodynamic sizes after 24 h incubation (Supporting Information, Figure S11). These results indicated that the PEG-PPS polymer based vesicles are naturally inert to the relatively low level of biologically relevant ROS.[20] TEM images confirmed that internal oxidation of the hydrophobic vesicular membrane after 8 Gy irradiation led to effective swelling and structural contraction which could facilitated the subsequent invasion and oxidation by external H_2O_2 (Figure 2d,e). The X-ray dose-dependent decomposition of the Au-LAHP-v was also studied by TEM images for two low doses of 4 and 6 Gy, respectively (Supporting Information, Figure S12). On the other hand, both the polymer only vesicles and Au-LA-v samples showed negligible morphological change in TEM images after X-ray even with a dose of 8 Gy (Supporting Information, Figure S13), indicating the critical role of localized •OH formation in destruction of vesicles upon X-ray irradiation.

Furthermore, U87MG cells were used to investigate the production of intracellular ROS indicated by 2',7'-ichlorodihydrofluorescein diacetate (H_2DCFDA). The results showed that X-ray alone was able to increase intracellular ROS level, while the presence of Au-LAHP-v, Au-LA-vDOX, and Au-LAHP-vDOX formulations further elevated ROS levels (Figure 3a). Remarkably, Au-LAHP-vDOX treated cells exhibited obvious accumulation of DOX in nucleus due to the instant release of free DOX after irradiation (Figure 3a, dotted square insets). In contrast, the fluorescence signal of DOX remained in cytosols of cells treated with Au-LA-vDOX. Semi-quantitative analysis showed that Au-LAHP-vDOX (+) led to an average of 4.7-fold increase of fluorescence intensity in cell nucleus over Au-LA-vDOX (+), illustrating the critical role of X-ray triggered release of DOX *in vitro*. Furthermore, the effective release of DOX and its active targeting to nucleus potentiate the improved cytotoxicity of Au-LA-vDOX (+) over others. Due to the possible additive effects of both generated •OH and released DOX upon irradiation, Au-LAHP-vDOX exerted the highest level of ROS in cells (Figure 3b and Supporting Information, Figure S14).

The cytotoxicity of different formulations with or without X-ray irradiation was then evaluated. Cells were treated with Au-LAHP-vDOX, Au-LAHP-v, Au-LA-vDOX, or free DOX at various concentrations normalized to the amount of DOX (or gold). At 24 h post-irradiation, Au-LAHP-vDOX exhibited the highest cytotoxicity compared with Au-LAHP-v and Au-LA-vDOX (Figure 3c). It is noteworthy that free DOX was still among the most potent drugs *in vitro* at 24 h post-irradiation, however, Au-LAHP-vDOX exhibited comparable cell cytotoxicity at 48 h post-irradiation for both 4 and 8 Gy irradiations

(Supporting Information, Figure S15). Flow cytometry assay indicated apoptotic or necrotic cell death especially for that treated with Au-LAHP-vDOX (Supporting Information, Figure S16). We further show that vDOX exhibited greatly diminished cytotoxicity compared with free DOX, indicating that a burst release of cargo drugs from the vesicles could be precluded (Supporting Information, Figure S17a,b). Additionally, the vesicles of polymers only and Au NPs exhibited little to no cytotoxicity (Supporting Information, Figure S17c,d). The potency of Au NPs serving as irradiation sensitizers showed concentration-dependent elevation of cytotoxicity for both single Au NPs and Au-LA-v vesicles (Supporting Information, Figure S18). Both the DNA double-strand breaks (DSBs) study and clonogenic assay showed that Au-LAHP-vDOX (+) resulted in the highest level of DNA damage and chronic cytotoxicity, which could be attributed to the synchronous chemoradiation effect (Supporting Information, Figure S19 and S20).

Prior to conducting the chemoradiation cancer therapy in mice, we studied the biodistribution of Au vesicles *in vivo* in a U87MG xenograft tumor mouse model by PET using ^{64}Cu as radiotracers.[21] The ^{64}Cu-Au vesicles were then intravenously injected into mice (n = 3) and the decay-correlated PET images were obtained at 1, 4, 24, and 48 h time points post-injection (p.i.) **(**Figure 4a**)**. The quantitative analysis of three-dimensional volume-of-interest showed a peak mean tumor uptake of 6.77 %ID/g at 24 h p.i., which dropped slightly to 5.9 %ID/g at 48 h p.i. (Supporting Information, Figure S21a). The *ex vivo* biodistribution results after 48 h p.i. were consistent with that derived from the PET images (Supporting Information, Figure S21b-d). It is noteworthy that little PET signal was recorded on mice kidneys and bladder, indicating good stability of the Au vesicles *in vivo*.

Furthermore, *in vivo* chemoradiation therapy was conducted in a subcutaneous mouse tumor model with normalized dosage of DOX of 4.0 mg/kg (n = 5/group). X-ray irradiation (8 Gy) was applied at 24 h p.i. for different groups. It was shown that the tumor growth of mouse groups receiving X-ray irradiation were significantly delayed (Figure 4b, grey and blue). In addition, Au-LA-vDOX (+) further inhibited tumor growth, which could be due to the good accumulation and retention effect in tumors and subsequently the slow release of DOX from the vesicles despite being unresponsive to irradiation (Figure 4b, green). This phenomenon was similar to that of Au-LAHP-vDOX treated mouse group without irradiation (Figure 4b, orange). In another set of cancer therapy experiment, eight groups including Au-LA-v, vDOX, free DOX, and PBS control with or without X-ray were studied (Supporting Information, Figure S22). The results indicated that (i) Au vesicles showed considerable radiation sensitizing effect with enhanced tumor growth inhibition compared with that of PBS plus X-ray group; (ii) concurrent chemoradiation for the vDOX plus X-ray group showed greater anti-cancer effect among others. Remarkably, under irradiation, Au-LAHP-vDOX treated mouse group showed continuous shrinkage of the tumor volume (Figure 4b, red). The quantitative percentage (%) of tumor volume inhibition at 20 days post-treatment showed a remarkable efficicacy (99.7%) for the mouse group treated with Au-LAHP-vDOX (+) over other groups. Three in five mice in this group were cured with no tumor recurrence and all the mice (except for sacrificing for tissue examinations) were alive until at least 50 days after irradiation (Supporting Information, Figure S23). The hematoxylin and eosin (H&E) staining results indicated little chronic toxicity to major organs after 20 days

(Supporting Information, Figure S24). The tumor cells of control showed densely distributed with large and deeply stained nuclei in the H&E staining image, which had clear and regular shaped nucleoli from the TEM image (Figure 4c). However, nuclei distortion and shrinkage, chromatin migration and fragmentation, and apoptotic bodies were observed in X-ray treated mouse, which was more prominent in the mouse tumor treated with Au-LAHP-vDOX (+) compared with other groups (Figure 4c and Supporting Information, Figure S25).

In conclusion, we have developed a novel nanovesicle consisting of X-ray irradiation labile LAHP molecules and oxidation-responsive PPS-PEG polymers, in which hydrophilic drugs DOX were loaded in the inner core of the Au-LAHP-vDOX vesicles. The release of cargo drugs is confined instantly when irradiation is applied to the Au-LAHP-vDOX owing to the *in situ* formation of •OH and the internal oxidation and efficient degradation of the vesicles. The established synchronous chemoradiation therapy showed impressive anticancer efficacy both *in vitro* and *in vivo*. In a subcutaneous mouse tumor model, three in five mice were cured without recurrence by one-dose injection and one-time X-ray irradiation. This study provides a paradigm of propagating concurrent chemoradiation into synchronous chemoradiation for effective cancer therapy, which may shed light on innovation of anticancer agents and strategies.

Supplementary Material

Refer to Web version on PubMed Central for supplementary material.

Acknowledgements

This work was supported by the Intramural Research Program (IRP), National Institute of Biomedical Imaging and Bioengineering (NIBIB), National Institutes of Health (NIH).

References

[1]. Zarin DA, Tse T, Sheehan New Engl J *J. Med.* 2015, 372, 174–180.

[2] (a). Webster RM, Nat. Rev. Drug Discov 2016, 15, 81–82 [PubMed: 26837588] (b)Komarova NL, Boland CR, Nature 2013, 499, 291–292 [PubMed: 23868257] (c)Chen H, Zhang W, Zhu G, Xie J, Chen X, Nat. Rev. Mater 2017, 2, 17024. [PubMed: 29075517]

[3]. Lopez JS, Banerji U, *Nat. Rev. Clin. Oncol.* 2017, 14, 57–66. [PubMed: 27377132]

[4] (a). Curran JWJ, Paulus R, Langer CJ, Komaki R, Lee JS, Hauser S, Movsas B, Wasserman T, Rosenthal SA, Gore E, Machtay M, Sause W, Cox JD, *J. Natl. Cancer Inst.* 2011, 103, 1452–1460 [PubMed: 21903745] (b)Forastiere AA, Goepfert H, Maor M, Pajak TF, Weber R, Morrison W, Glisson B, Trotti A, Ridge JA, Chao C, Peters G, Lee D-J, Leaf A, Ensley J, Cooper New Engl J *J. Med.* 2003, 349, 2091–2098.

[5] (a). Pignon JP, Bourhis J, Domenge C, Designé L, Lancet 2000, 355, 949–955 [PubMed: 10768432] (b)Tobias JS, Monson K, Gupta N, MacDougall H, Glaholm J, Hutchison I, Kadalayil L, Hackshaw A, Lancet Oncol. 2009, 11, 66–74. [PubMed: 19875337]

[6] (a). Song G, Cheng L, Chao Y, Yang K, Liu Z, *Adv. Mater.* 2017, 29, 201700996(b)Goel S, Ni D, Cai W, ACS Nano 2017, 11, 5233–5237; [PubMed: 28621524] (c)Fan W, Yung B, Huang P, Chen X, *Chem. Rev.* 2017, 117, 13566–13638. [PubMed: 29048884]

[7] (a). Zhang Y, Yin Q, Yin L, Ma L, Tang L, Cheng J, *Angew. Chem. Int. Ed.* 2013, 52, 6435–6439(b)Li X, Zheng B-Y, Ke M-R, Zhang Y, Huang J-D, Yoon J, Theranostics 2017, 7, 2746–2756 [PubMed: 28819460] (c)Lukianova-Hleb EY, Ren X, Sawant RR, Wu X, Torchilin VP, Lapotko DO, *Nat. Med.* 2014, 20, 778. [PubMed: 24880615]

[8] (a). Lu Y, Aimetti AA, Langer R, Gu Z, *Nat.* Rev. Mater. 2016, 2, 16075(b)Mura S, Nicolas J, Couvreur P, *Nat. Mater*. 2013, 12, 991–1003 [PubMed: 24150417] (c)Torchilin VP, *Nat. Rev. Drug Discov*. 2014, 13, 813–827. [PubMed: 25287120]

[9] (a). Chen B, Dai W, He B, Zhang H, Wang X, Wang Y, Zhang Q, Theranostics 2017, 7, 538–558 [PubMed: 28255348] (b)Dai Y, Xu C, Sun X, Chen X, *Chem. Soc. Rev*. 2017, 46, 3830–3852. [PubMed: 28516983]

[10] (a). Xu X, Saw PE, Tao W, Li Y, Ji X, Bhasin S, Liu Y, Ayyash D, Rasmussen J, Huo M, Shi J, Farokhzad OC, *Adv. Mater*. 2017, 29, 201700141(b)Li F, Li T, Sun C, Xia J, Jiao Y, Xu H, *Angew. Chem. Int. Ed*. 2017, 56, 10042–10046.

[11]. Wang Y, Kohane DS, *Nat. Rev. Mater*. 2017, 2, 17020.

[12] (a). Cao W, Zhang X, Miao X, Yang Z, Xu H, *Angew. Chem. Int. Ed*. 2013, 52, 6233–6237(b)Liu F, Lou J, Hristov D, Nanoscale 2017, 9, 14627–14634 [PubMed: 28936509] (c)Fan W, Bu W, Zhang Z, Shen B, Zhang H, He Q, Ni D, Cui Z, Zhao K, Bu J, Du J, Liu J, Shi J, *Angew. Chem. Int. Ed*. 2015, 54, 14026–14030.

[13] (a). Saravanakumar G, Kim J, Kim WJ, Adv. Sci 2017, 4, 1600124(b)Lv W, Zhang Z, Zhang KY, Yang H, Liu S, Xu A, Guo S, Zhao Q, Huang W, *Angew. Chem. Int. Ed*. 2016, 55, 9947–9951.

[14]. Cerritelli S, O'Neil CP, Velluto D, Fontana A, Adrian M, Dubochet J, Hubbell JA, Langmuir 2009, 25, 11328–11335. [PubMed: 19711914]

[15]. de Gracia Lux C, Joshi-Barr S, Nguyen T, Mahmoud E, Schopf E, Fomina N, Almutairi A, *J. Am. Chem. Soc*. 2012, 134, 15758–15764. [PubMed: 22946840]

[16] (a). Napoli A, Valentini M, Tirelli N, Mulle Mr, Hubbell JA, Nat. Mater 2004, 3, 183–189 [PubMed: 14991021] (b)Herzberger J, Fischer K, Leibig D, Bros M, Thiermann R, Frey H, *J. Am. Chem. Soc*. 2016, 138, 9212–9223. [PubMed: 27375132]

[17]. Holohan C, Van Schaeybroeck S, Longley DB, Johnston PG, Nat. Rev. Cancer 2013, 13, 714–726. [PubMed: 24060863]

[18] (a). Zhou Z, Song J, Tian R, Yang Z, Yu G, Lin L, Zhang G, Fan W, Zhang F, Niu G, Nie L, Chen X, Angew. Chem. Int. Ed. 2017, 56, 6492–6496(b)Zhou Z, Song J, Nie L, Chen X, *Chem. Soc. Rev*. 2016, 45, 6597–6626 [PubMed: 27722328] (c)Retif P, Pinel S, Toussaint M, Frochot C, Chouikrat R, Bastogne T, Barberi-Heyob M, Theranostics 2015, 5, 1030–1044. [PubMed: 26155318]

[19]. Napoli A, Tirelli N, Kilcher G, Hubbell A, Macromolecules 2001, 34, 8913–8917.

[20]. Allen BL, Johnson JD, Walker JP, ACS Nano 2011, 5, 5263–5272. [PubMed: 21595444]

[21]. Sun X, Huang X, Yan X, Wang Y, Guo J, Jacobson O, Liu D, Szajek LP, Zhu W, Niu G, Kiesewetter DO, Sun S, Chen X, ACS Nano 2014, 8, 8438–8446. [PubMed: 25019252]

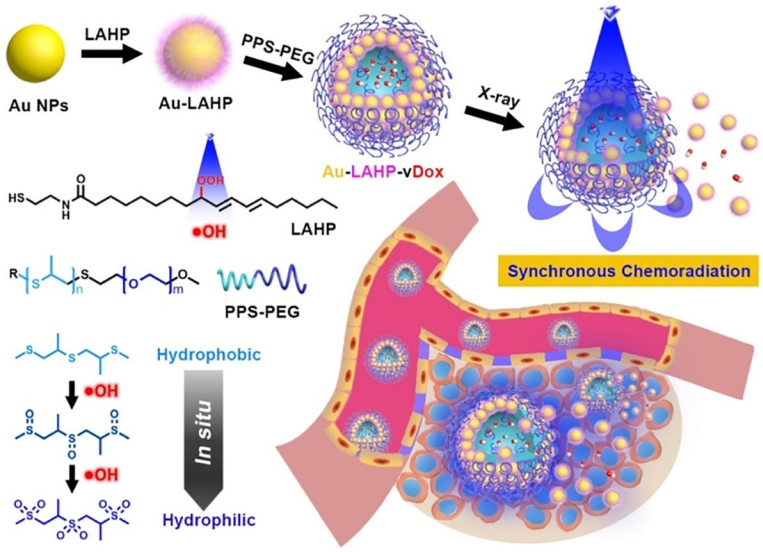

Figure 1.

Illustration of the synchronous chemoradiation. The co-assembly of hydrophobic Au-LAHP NPs, oxidation-responsive PPS-PEG amphiphilic polymers, and hydrophilic DOX result in Au-LAHP-vDOX vesicles. Upon irradiation, the *in situ* formation of •OH triggers oxidation of PPS from hydrophobic to hydrophilic, leading to degradation of the vesicles and burst release of cargo drugs. Therefore, drug release is synchronously confined when irradiation is applied in a spatiotemporally controllable manner.

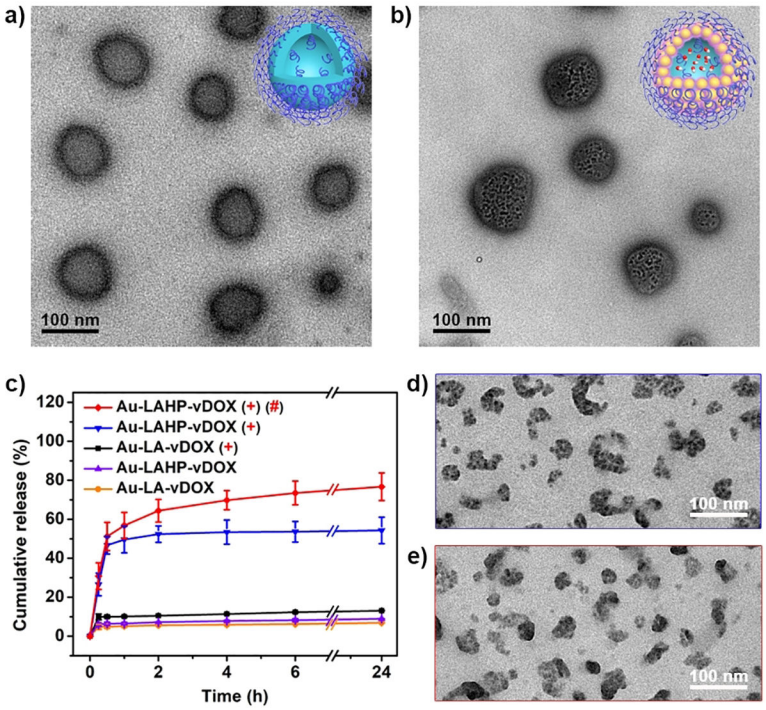

Figure 2.

TEM images of (a) PPS-PEG only and (b) Au-LAHP-vDOX vesicles. (c) Cumulative drug releasing profiles of the vesicles under different conditions. (+) represents that samples were applied with X-ray irradiation (8 Gy) and incubated with PBS (1×), (#) represents that sample was incubated with H_2O_2 (100 μM). TEM images of Au-LAHP-vDOX incubated with (d) PBS (1×) and (e) H_2O_2 (100 μM) after X-ray irradiation, respectively.

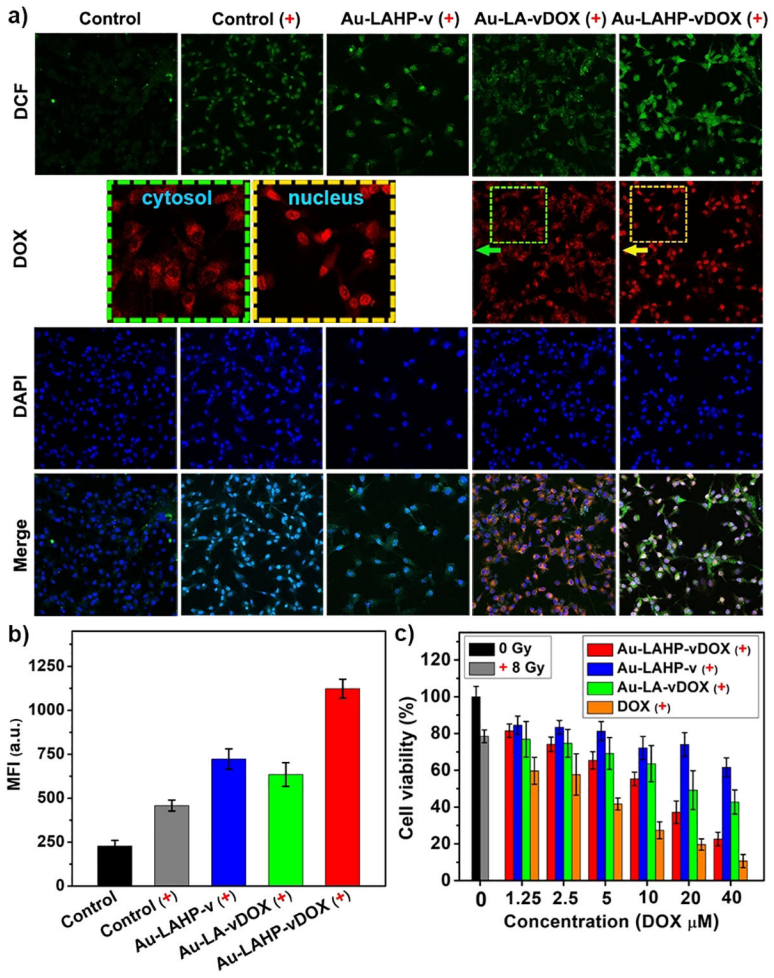

Figure 3.

(a) Confocal microscopy images of cells with different treatments. (+) represents that cells were applied with X-ray irradiation (8 Gy) before fixation. Magnified images of DOX signal channels show different locations of DOX at cytosol and nucleus, indicating little release and substantial release of DOX from Au-LA-vDOX (+) and Au-LAHP-vDOX (+), respectively. (b) Quantitative median fluorescence intensity (MFI) of DCF in cells with different treatments. (c) Cell viability assay on U87 MG cells 24 h after incubating with different formulations and X-ray irradiation (8 Gy). The concentrations were normalized to those of DOX (or gold) included.

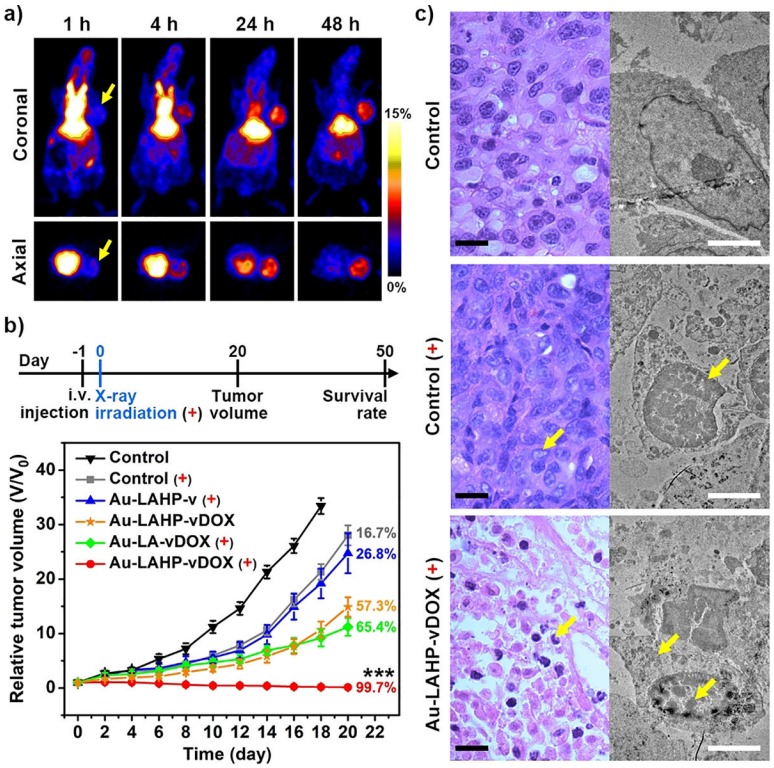

Figure 4.

(a) PET images of Au vesicles radiolabeled with ^{64}Cu radiotracers at different time points. Yellow arrows indicate tumors. (b) Cancer therapy study in a subcutaneous mouse tumor model. X-ray irradiation (8 Gy) was applied 24 h after i.v. injection of different formulations, and mouse tumor volume and survival rate were recorded until 20 and 50 days post-irradiation, respectively ($n = 5$, $^{***}p < 0.001$). The numbers indicate the quantitative percentage (%) of tumor volume inhibition values for each group. (c) Representative H&E staining (left) and TEM images (right) show changes in morphologies and microstructures of tumors after different treatments. Scale bar: 20 μm (black, left) and 5 μm (white, right). Yellow arrows indicate distortion and shrinkage of nuclei or chromatin migration in H&E images, and nuclear condensation, chromatin fragmentation, or formation of apoptotic bodies in TEM images.